

Characterization of Anisotropic Gaussian Random Fields by Minkowski Tensors

Michael Andreas Klatt^{1,2,‡}, Max Hörmann¹ and Klaus Mecke¹

¹ Friedrich-Alexander-Universität Erlangen-Nürnberg (FAU), Institut für Theoretische Physik, Staudtstr. 7, 91058 Erlangen, Germany; ² Experimental Physics, Saarland University, Center for Biophysics, 66123 Saarbrücken, Germany

E-mail: michael.klatt@fau.de

29 November 2021

Abstract. Gaussian random fields are among the most important models of amorphous spatial structures and appear across length scales in a variety of physical, biological, and geological applications, from composite materials to geospatial data. Anisotropy in such systems can sensitively and comprehensively be characterized by the so-called Minkowski tensors from integral geometry.

Here, we analytically calculate the expected Minkowski tensors of arbitrary rank for the level sets of Gaussian random fields. The explicit expressions for interfacial Minkowski tensors are confirmed in detailed simulations. We demonstrate how the Minkowski tensors detect and characterize the anisotropy of the level sets, and we clarify which shape information is contained in the Minkowski tensors of different rank.

Using an irreducible representation of the Minkowski tensors in the Euclidean plane, we show that higher-rank tensors indeed contain additional anisotropy information compared to a rank two tensor. Surprisingly, we can nevertheless predict this information from the second-rank tensor if we assume that the random field is Gaussian. This relation between tensors of different rank is independent of the details of the model. It is, therefore, useful for a null hypothesis test that detects non-Gaussianities in anisotropic random fields.

Keywords: Gaussian random fields, anisotropy, Minkowski tensors, tensor valuations, irreducible representation, Gaussian random waves

‡ Present address: Institut für Theoretische Physik II: Weiche Materie, Heinrich-Heine-Universität Düsseldorf 40225 Düsseldorf, Germany

1. Shape analysis of anisotropic random fields

Intuitively speaking, a random field is a function with random functional values, see Fig. 1. More precisely, the random field assigns to each point in space a random variable, typically, such that the functional values of proximate points are correlated with each other [1–3]. Hence, random fields are versatile models that are essential to a broad range of fields in physics, including quantum mechanics [4], cosmology [5], and material sciences [6]. They can be used to model random intensities or temperature profiles [7–11], coarse-grained particle density profiles [12–16], rough surfaces [17–19], or electric field distributions [20–22], to name just a few examples.

The arguably most important class of random fields are Gaussian random fields [3, 23]. Their importance is essentially due to the central limit theorem because a sum of many independent and identically distributed fluctuations can, virtually always, be well approximated by a Gaussian random field. Moreover, Gaussian random fields are specified by only their first and second moments, which leads to simple and controllable models in applications. Gaussian random fields have been used to model, for example, chaotic quantum systems [4, 24], random speckle patterns in optics [25] microemulsions [26], rough surfaces [27–29], thin films [30], heterogeneous materials [6], sea waves [31], and prominently the density fluctuations in the early universe [5].

An efficient way to analyze the complex shape of realizations of (Gaussian) random fields and capture higher-point information beyond the two-point correlation function is to characterize the corresponding level sets. More precisely, the random field is turned into a two-phase medium via thresholding. The set of all points with a functional value below the threshold is called the *excursion set* [23]. The geometry of the excursion set is then typically studied as a function of the threshold. Notably, the “density profile” of a random field can thus also be used to model porous media [26, 32, 33].

Minkowski functionals from integral geometry (also known as intrinsic volumes) are a powerful set of shape descriptors of excursion sets [1, 2, 34]. They comprise all ‘additive shape information’ according to the Hadwiger theorem [35]. As robust and versatile structural characteristics of random spatial and planar structures, they have been successfully applied to a broad range of applications [34, 36], from astronomy [10, 11, 37–40] to rough surfaces [19, 30, 41], biological tissues [42, 43], or porous media [12, 44, 45].

There is a rich literature on the characterization of Gaussian excursion sets [3, 9, 20, 23, 46, 47]. Specifically, the Minkowski functionals (MFs) for isotropic Gaussian random fields have already been intensively studied, including mean values [1, 27, 48], second moments, and asymptotic distributions [49–55]. The MFs have also been extensively used to study whether the cosmic microwave background is a Gaussian random field, e.g., see [56–60].

There are considerably fewer studies of the anisotropy of Gaussian random fields. Examples include nonisotropic quantum systems [61], anisotropic heterogeneous materials [6, 62], friction and rough surfaces [28], the modeling of sea waves [31, 63], and the stochastic heat equation [64]. Fractal anisotropic Gaussian random fields and their

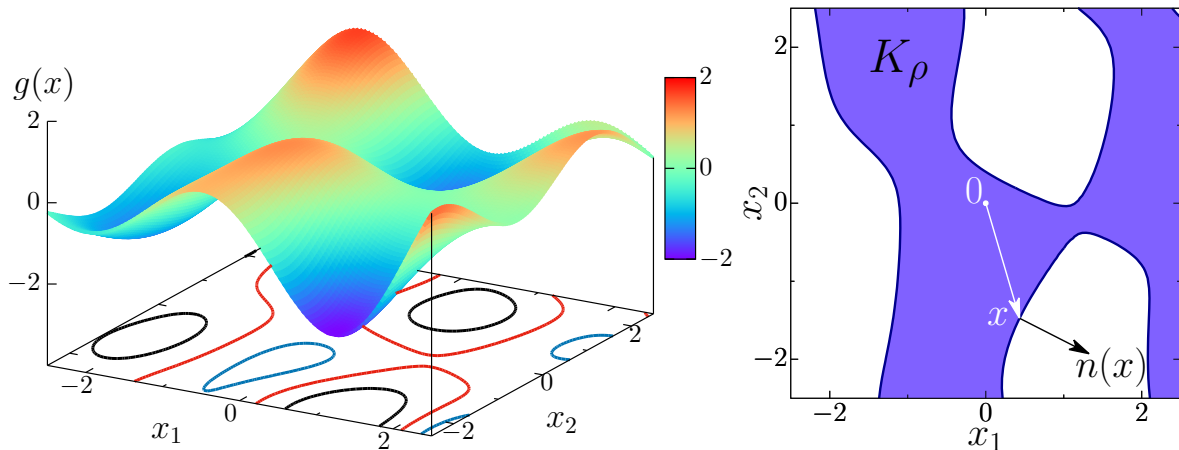


Figure 1. An exemplary realization of an anisotropic Gaussian random field $g(x)$ for $x = (x_1, x_2) \in \mathbb{R}^2$ is shown on the left hand side together with level sets for thresholds $\rho = -1, 0, 1$. On the right-hand side, the corresponding excursion set K_ρ is shown for $\rho = 0$. A normal vector $n(x)$ at a position x on the boundary is also depicted.

shape have been analyzed [62, 65] for models of porous materials [62] and biological tissues [66]. The mean values of MFs were also derived for anisotropic Gaussian random fields [1], and MFs were applied to analyze anisotropic porous materials [44] and surfaces [28].

The scalar MFs, however, do not directly detect or measure anisotropy, neither the degree nor the preferred direction. For this purpose, the MFs have been extended to the so-called Minkowski tensors (MTs) [67]. The MTs extend the notion of volume, surface area, and curvature to tensorial morphometric measures [34, 35, 68]. Thus, the MTs allow for a sensitive and comprehensive anisotropy analysis with respect to different geometrical properties, like surface area, circumference, or curvature [34, 35, 69–71]. Because they are robust against noise and their computation time grows linearly with the system size, they are efficient and comprehensive shape descriptors for data analysis of random spatial structures in experiments [34]. Minkowski tensors have already been successfully applied to a variety of experimental data sets, including solid foams [34, 72] and granular packings [73–76]. Recently, MTs were applied to analyze isotropic Gaussian random fields on the sphere and the cosmic microwave background [77–79], as well as two-dimensional slices of the dark matter density field [80], see also [81, 82].

Here, we use the MTs to characterize the anisotropy of Gaussian random fields [36, 83]; see Sec. 2 for a brief introduction to random fields and Minkowski tensors. We show how the MTs comprehensively detect and quantify anisotropy in general random fields, see Sec. 3. A key result is the mean-value formula for interfacial anisotropy of general smooth random fields in Eq. (21). We explicitly evaluate this formula for surface tensors of arbitrary rank and Gaussian random fields in arbitrary dimensions in Sec. 4, see Eq. (26).

We pay special attention to the question which information is contained in MT of different order and rank. Surprisingly, we find that while higher-rank MTs indeed

contain additional information, there is a strict relation between MT of different rank for a Gaussian random field independent of its correlation function. In fact, only assuming that the random field is Gaussian, MTs of arbitrary rank can be robustly predicted from the second-rank MT. A comparison of these predicted and measured values allows for a null hypothesis test that detects non-Gaussianities in anisotropic random fields. An outlook is given in Sec. 5.

We demonstrate the robustness of our MT analysis to finite-size effects and statistical noise by detailed simulations that accurately agree with our analytic predictions. Therefore, we define a class of parametric models with a tunable degree of anisotropy in Appendix A. Finally, we provide an introduction to *irreducible Minkowski tensors* (IMT) in Appendix B that is used in our analysis of Gaussian random fields, but that may be useful for more general planar random structures.

2. Background on random fields and Minkowski tensors

We here restrict our analysis to real-valued random fields that are defined on the Euclidean space \mathbb{R}^d . More precisely, such a random field can be defined as a collection of random variables so that it assigns to each site $x \in \mathbb{R}^d$ a real-valued random variable [1]. The functional value is sometimes called the ‘state’ of the system and x is a ‘site’, ‘index’, or ‘parameter’ [3]. In the following, we denote a realization of a general random field by a function $f(x)$ and that of a Gaussian random field by a function $g(x)$. We denote the corresponding random variables using capital letters, i.e., $F(x)$ and $G(x)$.

2.1. General random fields

The distribution of a random field F is specified by its *finite-dimensional distributions*, i.e., the joint distributions of $F(x_1), \dots, F(x_n)$ for all $x_1, \dots, x_n \in \mathbb{R}^d$ and all $n \in \mathbb{N}$. In the following, we assume that the random field is *statistically homogeneous* (or *stationary*), i.e., we assume that the finite-dimensional distributions are invariant under translations of the index set. Intuitively speaking, this implies that there is no preferred choice for the origin. A translation of the system does not change the statistical properties of the random field. Moreover, we assume that the fields are square-integrable (so that the first and second moments are well defined), ergodic, and sufficiently differentiable (so that all integral expressions are well defined, and limit operations can be exchanged).

Statistical homogeneity implies that the *mean function* of the random field $\mu(x) := \mathbb{E}[F(x)]$ is a constant for all $x \in \mathbb{R}^d$. Without loss of generality, we here choose $\mu(x) \equiv 0$. The *covariance function* of the random field F is then defined by:

$$\text{Cov}(x, y) := \mathbb{E}[F(x)F(y)] \quad (1)$$

for $x, y \in \mathbb{R}^d$. Because of the statistical homogeneity, $\text{Cov}(x, y)$ only depends on the difference of x and y , so that we can use the shorthand notation $\text{Cov}(x - y) := \text{Cov}(x, y)$. Since we are free to rescale the functional values, we here choose, again without loss

of generality, $\text{Var}[F(0)] = \text{Cov}(0) = 1$. The Fourier transformation of the covariance function is the *power spectral density*:

$$s(q) = \int_{\mathbb{R}^d} \text{Cov}(x) e^{-i\langle q, x \rangle} dx, \quad (2)$$

where $q \in \mathbb{R}^d$ is called the wave vector, and $\langle q, x \rangle$ denotes the scalar product.

Finally, we define the *excursion set* K_ρ for a given realization $f(x)$ of the random field F :

$$K_\rho := \{x \in \mathbb{R}^d \mid f(x) \geq \rho\}, \quad (3)$$

i.e., K_ρ is the set of all points x for which the functional value $f(x)$ is larger or equal to a given threshold ρ [23]. Its boundary $\partial K_\rho = f^{-1}(\rho)$ is known as a *level set*, see Fig. 1.

2.2. Gaussian random fields

If all finite-dimensional distributions are Gaussian, then the random field G is said to be a *Gaussian random field*. Recall that the distribution of a Gaussian random vector $Y \in \mathbb{R}^n$ is determined by its mean vector $\mu_Y := \mathbb{E}[Y]$ and covariance matrix $C_Y := \text{Cov}[Y]$. If C_Y is regular, then Y has the probability density

$$\varphi_Y(y) := \frac{1}{(2\pi)^{n/2} \sqrt{\det C_Y}} e^{-\frac{1}{2} \langle y - \mu_Y, C_Y^{-1} (y - \mu_Y) \rangle}. \quad (4)$$

Similar to a multivariate Gaussian distribution, the distribution of a stationary Gaussian random field is determined by μ and $\text{Cov}(x)$. For our choice of units, the probability density function of $G(0)$ is a standard normal distribution, i.e., centered and with unit variance.

For a smooth, centered Gaussian random field, the gradient $\nabla G(0)$ also has a centered Gaussian distribution [84, Corollary 4.4], see also [85, Lemma 2.3.6]. For a statistically homogeneous, differentiable random field, the functional value and the gradient are uncorrelated [1, Eq. (5.5.6)]. Hence they are even stochastically independent for a Gaussian random field G .

In the following, we study functionals $M : g \rightarrow \mathbb{R}$ that map the realization of a random field to a real number, like the volume of the intersection of an excursion set with an observation window. We denote the mean value of such a functional by $\mathbb{E}[M]$.

2.3. Minkowski tensors

Minkowski functionals (MF) and Minkowski tensors (MT) have a rigorous, mathematical foundation in integral geometry [1, 2, 35], which also offers insights for applications. For example, Hadwiger's theorem [86] guarantees that the MFs contain all additive scalar shape information (that is, any motion invariant functional that is additive and fulfills minor continuity requirements is a linear combination of MFs). This remarkable statement has been generalized to the MTs [87, 88]. Moreover, the MFs and MTs have

intuitive geometric interpretations, including volume, surface area, and moments of the distributions of mass or normal vectors [34, 71].

For a smooth, bounded domain $K \subset \mathbb{R}^d$, the MFs can be represented by integrals over the volume or as curvature-weighted integrals over the boundary ∂K , respectively:

$$W_0 := \int_K dx, \quad (5)$$

$$W_\nu := \int_{\partial K} H_{\nu-1}(K, x) dS(x), \quad \text{for } \nu = 1, \dots, d, \quad (6)$$

where dS denotes the $(d-1)$ -dimensional surface measure, and the $H_j(K, x)$ are the elementary symmetric polynomials of the *principal curvatures* $\kappa_1(K, x), \dots, \kappa_{d-1}(K, x)$ of K at $x \in \partial K$:

$$H_j(K, x) := \sum_{|I|=j} \prod_{l \in I} \kappa_l(K, x) \quad (7)$$

with the summation extending over all subsets $I \subset \{1, \dots, d-1\}$ of cardinality j and $H_0(K, x) = 1$. Different normalizing constants are used in different context. Here, we choose a normalization such that $W_1 = \int_{\partial K} dS(x)$ is the surface area (or circumference) of K .

The scalar MFs can naturally be generalized to tensors that quantify anisotropy, simply by multiplying the integrand with the symmetric tensor product $x^r n^s(x)$ of the position vector x and the normal vector $n(x)$ with $r, s \in \mathbb{N}$:

$$W_0^{r,0}(K) := \int_K x^r dx, \quad (8)$$

$$W_\nu^{r,s}(K) := \int_{\partial K} x^r n^s(x) H_{\nu-1}(K, x) dS(x), \quad \text{for } \nu = 1, \dots, d, \quad (9)$$

where the normal vector $n(x)$ is perpendicular to the (smooth) interface at position $x \in \partial K_\rho$ and pointing outwards, see Fig. 1. For a mathematical definition of the symmetric tensor product, e.g., see [89]. Here it suffices to focus on the tensors $W_0^{r,0}$ and $W_\nu^{0,s}$ and hence on the tensor product y^t of a single vector $y \in \mathbb{R}^d$ and $t \in \mathbb{N}$, for which the Cartesian representation is simply given by a matrix with entries $(y^t)_{j_1 \dots j_s} = y_{j_1} \dots y_{j_s}$.

The tensors $W_0^{r,0}$ quantify the distribution of mass in a homogeneous solid body. The tensors $W_\nu^{0,s}$ describe how the orientation of the interface is distributed, possibly weighted by the curvature of the interface. In contrast to $W_0^{r,0}$, the tensors $W_\nu^{0,s}$ are translation invariant.

3. Anisotropy quantification for general random fields

For a statistically homogeneous random field, we can study the Minkowski functionals and tensors of the excursion set K_ρ in the thermodynamic limit. More precisely, we first compute the mean value $\mathbb{E}[W_\nu^{r,s}(K_\rho \cap \Omega)]$ of a Minkowski tensor in a finite observation window $\Omega \subset \mathbb{R}^d$, then rescale the expectation with the size of the window, and finally

consider the thermodynamic limit:

$$w_\nu^{r,s}(\rho) := \lim_{|\Omega| \rightarrow \infty} \frac{\mathbb{E}[W_\nu^{r,s}(K_\rho \cap \Omega)]}{|\Omega|^{1+r/d}}, \quad (10)$$

where $|\Omega|$ is a shorthand notation for the volume $W_0(\Omega)$ of the observation window. The limit is a *Minkowski tensor density*. For example, the density of the volume is the well-known volume fraction $\phi(\rho)$ of the excursion set K_ρ :

$$\phi(\rho) := w_0^{0,0}(\rho) = \lim_{|\Omega| \rightarrow \infty} \frac{1}{|\Omega|} \mathbb{E} \left[\int_{\Omega} \mathbb{1}\{F(x) \geq \rho\} dx \right] \quad (11)$$

$$= \lim_{|\Omega| \rightarrow \infty} \int_{\Omega} \frac{1}{|\Omega|} \mathbb{E} [\mathbb{1}\{F(x) \geq \rho\}] dx \quad (12)$$

$$= \mathbb{E} [\mathbb{1}\{F(0) \geq \rho\}] \lim_{|\Omega| \rightarrow \infty} \int_{\Omega} \frac{1}{|\Omega|} dx \quad (13)$$

$$= \mathbb{P}[F(0) \geq \rho] \quad (14)$$

where $\mathbb{1}\{F(0) \geq \rho\}$ is the indicator function of the excursion set, and in the second to last line, we have taken advantage of the statistical homogeneity.

A key question is what information about the statistically homogeneous random field F is contained in volume-based or interfacial-based MTs, respectively? The answer for the volume-based MTs is straightforward since the calculation closely follows that of the volume:

$$w_0^{r,0}(\rho) = \lim_{|\Omega| \rightarrow \infty} \int_{\Omega} \frac{x^r}{|\Omega|^{1+r/d}} \mathbb{E} [\mathbb{1}\{F(x) \geq \rho\}] dx \quad (15)$$

$$= \phi(\rho) \lim_{|\Omega| \rightarrow \infty} \int_{\Omega} \frac{x^r}{|\Omega|^{1+r/d}} dx. \quad (16)$$

The only information about the Gaussian random field that is contained in the densities of the volume-based MTs of arbitrary rank is $\phi(\rho)$. The scalar volume fraction is simply multiplied by a rescaled MT of the observation window. An intuitive interpretation is that a statistically homogeneous random field cannot exhibit any anisotropy in the average distribution of “mass”.

This is to be contrasted to the anisotropy of the orientation of the interface or curvature, which is quantified by the interfacial-based MT densities. We here derive a general formula that expresses the global average of the MT densities by local averages of the functional values and gradient. Therefore, we neglect boundary contributions in the thermodynamic limit and apply the coarea formula [90] with $\partial K_\rho = F^{-1}(\rho)$, where we use the Dirac-delta notation:

$$w_\nu^{0,s}(\rho) = \lim_{|\Omega| \rightarrow \infty} \frac{1}{|\Omega|} \mathbb{E} \left[\int_{\Omega \cap \partial K_\rho} n^s(x) H_{\nu-1}(K_\rho \cap \Omega, x) dS(x) \right] \quad (17)$$

$$= \lim_{|\Omega| \rightarrow \infty} \frac{1}{|\Omega|} \mathbb{E} \left[\int_{\Omega} n^s(x) H_{\nu-1}(K_\rho \cap \Omega, x) \|\nabla F(x)\| \delta(F(x) - \rho) dx \right] \quad (18)$$

$$= \lim_{|\Omega| \rightarrow \infty} \frac{1}{|\Omega|} \int_{\Omega} \mathbb{E} \left[n^s(x) H_{\nu-1}(K_\rho \cap \Omega, x) \|\nabla F(x)\| \delta(F(x) - \rho) \right] dx \quad (19)$$

$$= \mathbb{E} \left[n^s(0) H_{\nu-1}(K_\rho \cap \Omega, 0) \|\nabla F(0)\| \delta(F(0) - \rho) \right]. \quad (20)$$

Since the gradient of a smooth function is always antiparallel to the normal vector on the excursion set, we obtain

$$w_\nu^{0,s}(\rho) = (-1)^s \mathbb{E} \left[H_{\nu-1}(K_\rho \cap \Omega, 0) (\nabla F(0))^s \|\nabla F(0)\|^{-s+1} \delta(F(0) - \rho) \right]. \quad (21)$$

Because of the additivity of the MT, we only need the distributions of the functionals value and derivatives at the origin to compute the global average of the MT. This is carried out in the following section for $w_1^{0,s}$ of the Gaussian random field. The calculations for $\nu > 1$ are technically more involved but follow the same principle.

4. Shape characterization of Gaussian random fields

For a Gaussian random field G , we can explicitly evaluate Eq. (21) for $\nu = 1$ since $G(0)$ and $\nabla G(0)$ are stochastically independent (see Sec. 2.2). The MT densities $w_1^{0,s}$ of Gaussian random fields in arbitrary dimensions are given by:

$$w_1^{0,s}(\rho) = (-1)^s \mathbb{E} \left[(\nabla G(0))^s \|\nabla G(0)\|^{-s+1} \delta(G(0) - \rho) \right] \quad (22)$$

$$= (-1)^s \int_{\mathbb{R}^d} \delta(g_0 - \rho) \varphi_{G(0)}(g_0) dg_0 \int_{\mathbb{R}^d} \frac{g_1^s}{\|g_1\|^{s-1}} \varphi_{\nabla G(0)}(g_1) dg_1 \quad (23)$$

$$= (-1)^s \varphi_{G(0)}(\rho) \int_{\mathbb{R}^d} \frac{g_1^s}{\|g_1\|^{s-1}} \varphi_{\nabla G(0)}(g_1) dg_1, \quad (24)$$

For tensors $w_1^{0,2s-1}$ of odd rank, the integrand in Eq. (24) is anti-symmetric. Hence, all interfacial MT densities of odd rank vanish:

$$w_1^{0,2s-1}(\rho) \equiv 0, \quad (25)$$

independent of the covariance functions of the Gaussian random field. A vanishing of all odd rank tensors implies a centrally symmetric distribution of the normal vectors, which is consistent with the fact that the covariance function is centrally symmetric.

The interfacial anisotropy is, therefore, exclusively encoded in the even rank tensors. By expressing the remaining integral in Eq. (24) in spherical coordinates, we can carry out the integration of the absolute value of the gradient so that only the integration of the direction $u \in \mathbb{S}^{d-1}$ of the gradient remains. For tensors of even rank s , we thus obtain:

$$w_1^{0,s}(\rho) = \varphi_{G(0)}(\rho) \frac{2^{(d-1)/2} \Gamma((d+1)/2)}{(2\pi)^{d/2} \sqrt{\det C_{\nabla G(0)}}} \int_{\mathbb{S}^{d-1}} \frac{u^s}{\langle u, C_{\nabla G(0)}^{-1} u \rangle^{(d+1)/2}} du, \quad (26)$$

where $C_{\nabla G(0)}$ is the covariance matrix of $\nabla G(0)$ and Γ is the gamma function.

Remarkably, the MT densities $w_1^{0,s}(\rho)$ only trivially depend on the threshold ρ via a scalar prefactor $\varphi_{G(0)}(\rho)$. In other words, the choice of the threshold only changes the trace of the tensor $w_1^{0,s}(\rho)$, which is, in fact, the specific surface $w_1^{0,0}(\rho)$. In contrast, the actual anisotropy information encoded in the higher rank tensors is independent of ρ . This implies that the degree of anisotropy and the preferred orientation are intrinsic properties of the Gaussian random field. Note that this holds for all tensor densities $w_\nu^{0,s}(\rho)$ with $\nu > 0$.

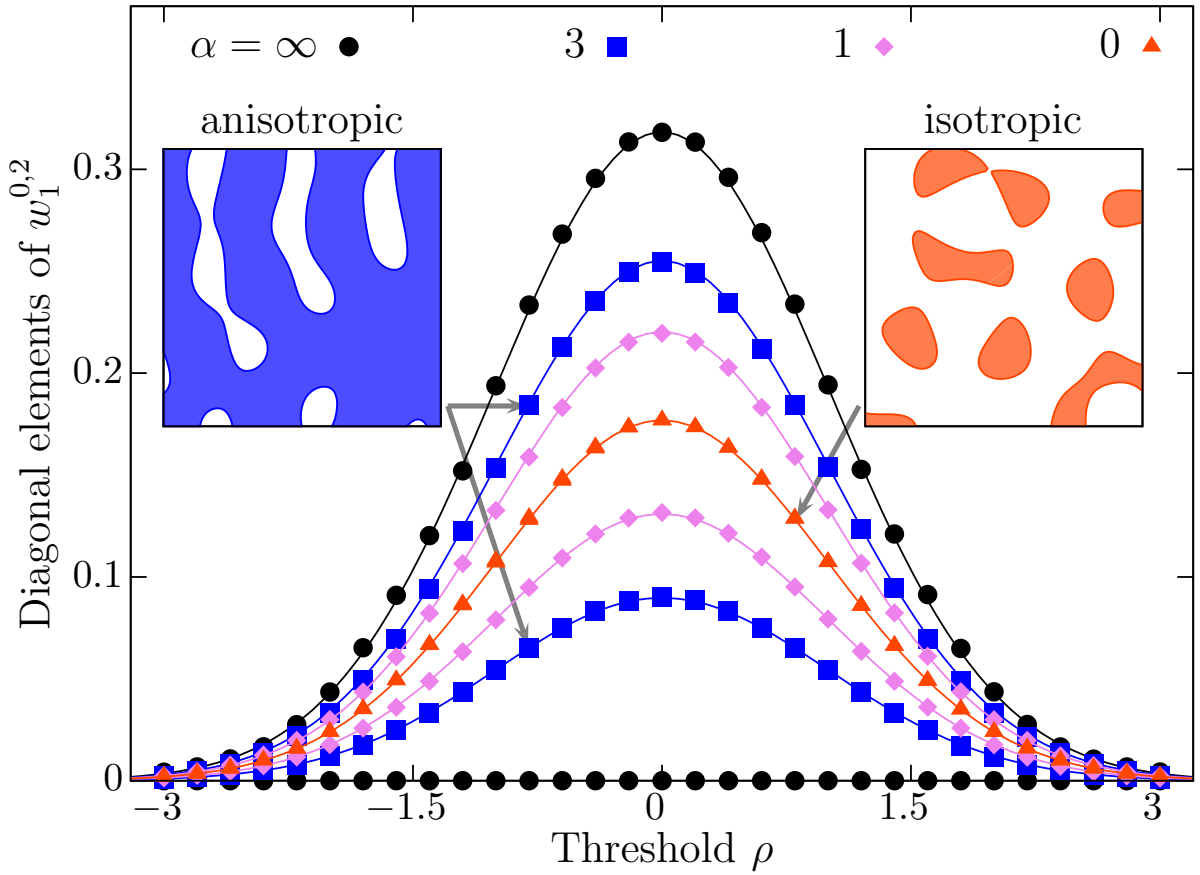


Figure 2. The diagonal elements of the MT density $w_1^{0,2}$ in the Cartesian representation for a Gaussian random field as a function of the threshold ρ , see Eq. (28), for differently anisotropic Gaussian random wave models.

4.1. Planar Gaussian random fields

Because the covariance matrix $C_{\nabla G(0)}$ is symmetric, a rotation, represented by a rotation matrix Q , can diagonalize the covariance matrix. Using the Cartesian representation, we can write in two dimensions

$$C_{\nabla G(0)} = Q \begin{pmatrix} \lambda_1 & 0 \\ 0 & \lambda_2 \end{pmatrix} Q^t. \quad (27)$$

Thus, the integral in Eq. (26) can be easily calculated, e.g., for the second-rank tensor:

$$w_1^{0,2}(\rho) = \varphi_{G(0)}(\rho) \sqrt{\frac{2}{\pi} \frac{\sqrt{\lambda_1 \lambda_2}}{\lambda_2 - \lambda_1}} Q \begin{pmatrix} h(\lambda_1, \lambda_2) & 0 \\ 0 & -h(\lambda_2, \lambda_1) \end{pmatrix} Q^t \quad (28)$$

with

$$h(x, y) := \sqrt{x} \left[K \left(1 - \frac{x}{y} \right) - E \left(1 - \frac{x}{y} \right) \right], \quad (29)$$

where $K(k)$ and $E(k)$ are the complete elliptic integral of the first and second kind, respectively.

To exemplify the behavior of the MT densities, we define a class of parametric Gaussian random wave models, in which we can tune the degree of anisotropy from an isotropic ($\alpha = 0$) to a “completely anisotropic” model ($\alpha = \infty$). In the latter case, the excursion sets are effectively one-dimensional and consist of parallel slabs with varying thicknesses. The class of models is defined in detail in Appendix A. There we also describe the simulation procedure and parameters.

Figure 2 shows the diagonal elements of the tensor $w_1^{0,2}$ in the Cartesian representation as a function of the threshold ρ . The lines depict the analytic curves. The points show numerical estimates from simulated random fields, which are in excellent agreement with the exact results. For the isotropic system, the diagonal elements coincide $(w_1^{0,2})_{xx} = (w_1^{0,2})_{yy} = \frac{1}{2}w_1^{0,0}$. As the degree of anisotropy increases, $(w_1^{0,2})_{xx}$ increases and $(w_1^{0,2})_{yy}$ decreases. For an effectively one-dimensional model with $\alpha = \infty$, $(w_1^{0,2})_{yy}$ vanishes.

4.2. Additional anisotropy information in higher-rank tensors

Assuming a diagonal covariance matrix of the gradient, also the fourth rank tensor can be calculated straightforwardly (for $\lambda_2 > 0$)

$$(w_1^{0,4})_{xxxx} = \varphi_{G(0)}(\rho) \sqrt{\frac{2}{\pi}} \frac{\lambda_1 \left((\lambda_1 + \lambda_2) E\left(1 - \frac{\lambda_1}{\lambda_2}\right) - 2\lambda_1 K\left(1 - \frac{\lambda_1}{\lambda_2}\right) \right)}{\lambda_2 \sqrt{\lambda_2} \left(1 - \frac{\lambda_1}{\lambda_2}\right)^2}, \quad (30)$$

$$(w_1^{0,4})_{yyyy} = \frac{\lambda_2}{\lambda_1} (w_1^{0,4})_{xxxx}, \quad (31)$$

$$(w_1^{0,4})_{xxyy} = (w_1^{0,2})_{xx} - (w_1^{0,4})_{xxxx}, \quad (32)$$

$$(w_1^{0,4})_{xyyy} = (w_1^{0,4})_{xxyy} = 0. \quad (33)$$

In the Cartesian representation, it is non-trivial to check whether the fourth-rank tensor contains additional anisotropy information compared to the second-rank tensor. We, therefore, switch to the irreducible representation, which is explained in detail in Appendix B.

There we derive from the irreducible representation with respect to $\text{SO}(2)$ scalar anisotropy indices $q_s \in [0, 1]$ that characterize the degree of anisotropy. If $q_s > 0$, anisotropy is detected by the tensor of rank s that is not captured by tensors of another rank. Explicit expressions for the irreducible anisotropy indices q_2 and q_4 can be derived for planar Gaussian random fields by inserting Eqs. (28) and (33) into Eqs. (B.10) and (B.11).

The resulting data for our Gaussian random waves models are plotted in Fig. 3. As before, the lines depict the analytic curves, and the points represent the simulation results, which are again in excellent agreement with the formulas. Since the degree of anisotropy is, as explained above, an inherent property of the Gaussian random field, the anisotropy indices are independent of the threshold ρ . Importantly, we find that $q_4 > 0$ for anisotropic Gaussian random fields, i.e., the tensor of rank four captures additional anisotropy information that is not contained in the second-rank tensor.

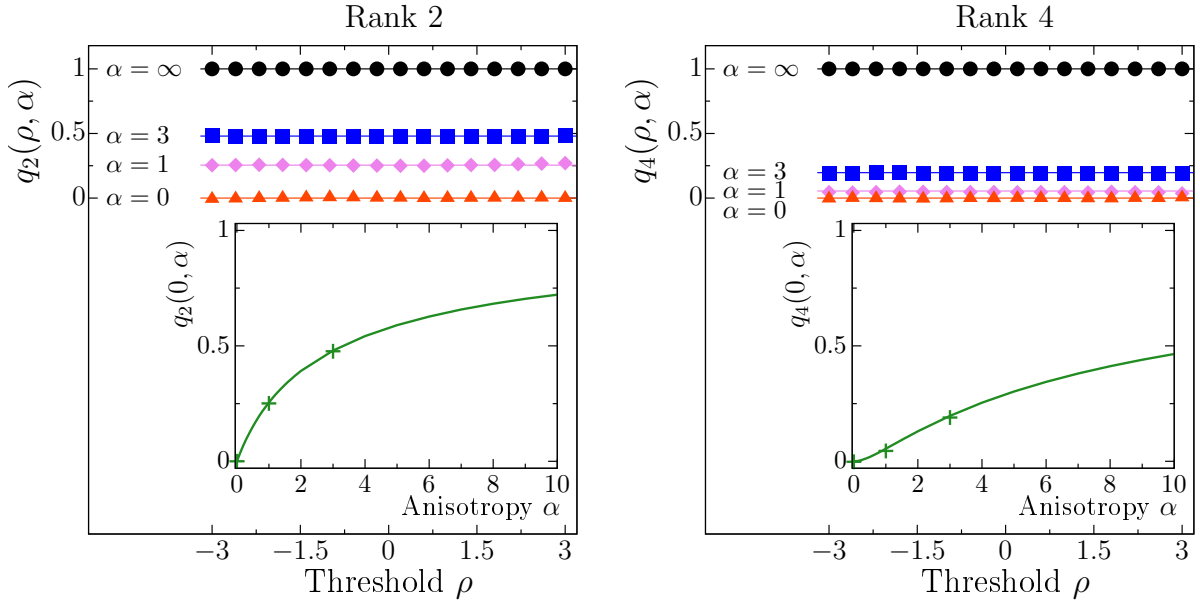


Figure 3. Anisotropy indices of rank two and four for differently anisotropic Gaussian random wave models: The indices q_2 and q_4 are the ratio of the absolute value of the irreducible representations of rank 2 and rank 0 or rank 4 and rank 0, respectively, see Eqs. (B.10) and (B.11). The indices as a function of the threshold ρ are constant, that is, independent of ρ . The insets show the indices as a function of the anisotropy parameter α of the models. Because $q_4 > 0$, the fourth rank tensor $w_1^{0,4}$ contains nonredundant anisotropy information compared to the second-rank tensor.

4.3. Higher-rank tensors predicted from second-rank tensors

What this example demonstrates is that higher-rank tensors of Gaussian random fields will generally contain additional anisotropy information. The next question is: what kind of additional information is contained in the higher-rank tensors?

To answer this question, we express the MTs $W_1^{0,s}(K)$ as moment tensors of the distribution of its normal vectors, or more precisely, of its extended Gaussian image Ψ_K , as in Appendix B:

$$W_1^{0,s}(K) = \int_{\mathbb{S}^{d-1}} u^s \Psi_K(u) du \text{ with } \Psi_K(u) := \int_{\partial K} \delta(n(x) - u) dS(x). \quad (34)$$

The MT densities follow from a corresponding density $\psi(u, \rho)$ of the EGI:

$$\psi(u, \rho) := \lim_{|\Omega| \rightarrow \infty} \frac{\mathbb{E}[\Psi_{K_\rho \cap \Omega}(u)]}{|\Omega|} \quad (35)$$

where $u \in \mathbb{S}^{d-1}$. In analogy to Eqs. (17)–(20), we derive for a general random field F

(subject to our assumptions in Sec. 2):

$$\psi(u, \rho) = \lim_{|\Omega| \rightarrow \infty} \frac{1}{|\Omega|} \mathbb{E} \left[\int_{\Omega \cap \partial K} \delta(n(x) - u) dS(x) \right] \quad (36)$$

$$= \lim_{|\Omega| \rightarrow \infty} \frac{1}{|\Omega|} \mathbb{E} \left[\int_{\Omega} \delta(n(x) - u) \|\nabla F(x)\| \delta(F(x) - \rho) dx \right] \quad (37)$$

$$= \lim_{|\Omega| \rightarrow \infty} \frac{1}{|\Omega|} \int_{\Omega} \mathbb{E} [\delta(n(x) - u) \|\nabla F(x)\| \delta(F(x) - \rho)] dx \quad (38)$$

$$= \mathbb{E} [\delta(n(0) - u) \|\nabla F(0)\| \delta(F(0) - \rho)]. \quad (39)$$

For a Gaussian random field G , we obtain more explicitly—in analogy to the derivation of Eq. (24):

$$\psi(u, \rho) = \mathbb{E} \left[\delta \left(\frac{\nabla G(0)}{\|\nabla G(0)\|} + u \right) \|\nabla G(0)\| \right] \mathbb{E} [\delta(G(0) - \rho)] \quad (40)$$

$$= \varphi_{G(0)}(\rho) \int_{\mathbb{R}^d} \delta \left(\frac{g_1}{\|g_1\|} + u \right) \|g_1\| \varphi_{\nabla G(0)}(g_1) dg_1 \quad (41)$$

For a Gaussian random field, the interfacial anisotropy depends on the threshold only via a scalar prefactor, as discussed above. To evaluate the remaining integral, we separate the integral over the absolute value $\gamma_1 := \|g_1\|$ and direction $n_1 := g_1/\|g_1\|$ of the gradient:

$$\psi(u, \rho) = \varphi_{G(0)}(\rho) \int_{\mathbb{R}} \gamma_1^d \int_{\mathbb{S}^{d-1}} \delta(n_1 + u) \varphi_{\nabla G(0)}(\gamma_1 n_1) dn_1 d\gamma_1 \quad (42)$$

$$= \varphi_{G(0)}(\rho) \int_{\mathbb{R}} \gamma_1^d \varphi_{\nabla G(0)}(\gamma_1 u) d\gamma_1, \quad (43)$$

where we have used the symmetry of $\varphi_{\nabla G(0)}$ in the last equation. Inserting the Gaussian probability density function of the gradient yields the explicit expression for the EGI density in any dimension d :

$$\psi(u, \rho) = \varphi_{G(0)}(\rho) \frac{2^{(d-1)/2} \Gamma((d+1)/2)}{(2\pi)^{d/2} \sqrt{\det C_{\nabla G(0)}}} \times \frac{1}{\langle u, C_{\nabla G(0)}^{-1} u \rangle^{(d+1)/2}}. \quad (44)$$

Exemplary curves of $\psi(u, \rho)$ are shown in Fig. 4 for our parametric Gaussian random wave model. For the isotropic system, the polar plot forms a circle. For the anisotropic systems, the curves are dumbbell-shaped. The more anisotropic the field, the more anisotropic the polar plot is, i.e., more normal vectors are pointing in the horizontal than in the vertical direction.

The MT densities of arbitrary rank easily follow from the EGI density because the averaging of the MT and the limit are linear operations. Therefore, Eq. (34) can be directly transferred to the densities:

$$w_1^{0,s}(\rho) = \int_{\mathbb{S}^{d-1}} u^s \psi(u, \rho) du. \quad (45)$$

Note the agreement with Eq. (26).

Now we can return to the question of what kind of additional information is contained in the higher-rank tensors? Equation (44) shows that the information about

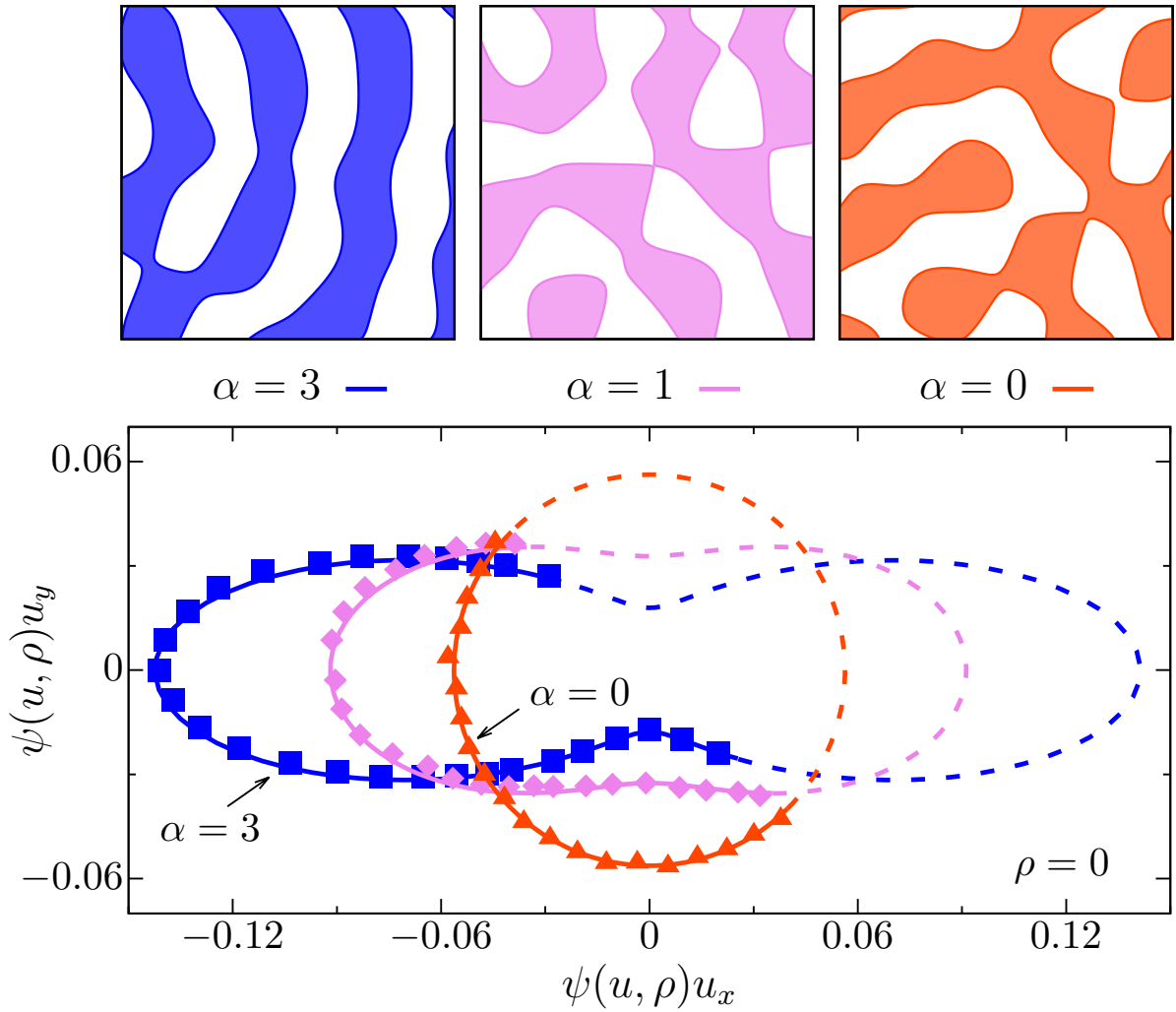


Figure 4. The EGI density $\psi(u, \rho)$ from Eq. (44) is shown for Gaussian random wave models with different degrees of anisotropy (from isotropic $\alpha = 0$ to strongly anisotropic $\alpha = 3$). At the top, samples of the excursion sets are depicted. The main figure is a polar plot of the EGI densities. The solid lines show the analytic curves, which are compared to the direct numerical estimates of $\psi(u, \rho)$ represented by the marks, which are in very good agreement with the prediction from the formula. The dashed lines correspond to estimates of the EGI density that are based only on the measurement of $w_1^{0,2}$ (via the method of moments). This estimate is in even better agreement with the analytic curves. (Note that the polar plot of $\psi(u, \rho)$ is point symmetric with respect to the origin.)

the Gaussian random field that is encoded in the EGI density and thus in all MT densities is the covariance matrix $C_{\nabla G(0)}$ of the gradient at the origin (and the variance of the functional value, which is determined by the choice of units). From the derivation, we can conclude that the underlying reason for this parametrization of $\psi(u, \rho)$ via $C_{\nabla G(0)}$ is the stationarity of the random field together with the additivity of the MT. For that reason, the EGI density only depends on the distributions of the functional value and the gradient of the Gaussian random field at the origin, see Eq. (39). Because both

are centered Gaussian distributions, they are entirely determined by their variances and covariances.

The essential information about the Gaussian random field, which is encoded in the tensors, is thus the covariance matrix $C_{\nabla G(0)}$. Because it is a symmetric second-rank tensor, its elements can actually be estimated from the second-rank MT density $w_1^{0,2}$. Note that this can already be deduced from Eq. (26). Still, the EGI density offers a more transparent presentation, and we employ it in the following to demonstrate that by measuring $w_1^{0,2}$, we can robustly estimate the EGI density and thus all higher-rank tensors of the Gaussian random field.

We, therefore, apply the method of moments exemplarily in two dimensions. First, we numerically solve Eq. (28) for the eigenvalues λ_1 and λ_2 of $C_{\nabla G(0)}$. Then, we numerically estimate $w_1^{0,2}$ based on 3000 samples of excursion sets of the Gaussian random wave models from Fig. 4 at threshold $\rho = 0$. We then use the eigenvectors of $w_1^{0,2}$ to determine the rotation matrix Q . Using the ratio of the eigenvalues, we then estimate the ratio of λ_1 and λ_2 . Finally, we use the trace of $w_1^{0,2}$ to estimate the absolute values of λ_1 and λ_2 .

To confirm the outcome, we insert the estimated \hat{Q} , $\hat{\lambda}_1$, and $\hat{\lambda}_2$ in Eq. (44) and plot the resulting curve for $\psi(u, \rho)$ in Fig. 4 (dashed lines). It is in excellent agreement with the exact analytic curve of the EGI density (solid line). The statistical errors are distinctly smaller than for the points that represent the direct estimate of $e(u, \rho)$ for some directions u (based on a data set twice as large). The second-rank MT density suffices for a robust and accurate estimate of the EGI density and, thus, all higher-rank tensors.

At first, it might sound like a contradiction that, on the one hand, higher-rank tensors contain additional information, as we discovered in the previous section, but that, on the other hand, we have now predicted this additional information from the second-rank tensor. The key difference is that in the previous section, we did not have to assume that the random field is Gaussian to compute the anisotropy indices q_s and thus extract additional information. In contrast, our prediction of the higher-rank tensors is only valid for Gaussian random fields.

Let us illustrate this finding with an elucidating geometrical analogy: the anisotropy of a rectangle. If we only know the second-rank tensor of a convex body, we cannot reconstruct its shape without further prior knowledge. The infinite series of interfacial MTs $W_1^{0,s}$ is needed to reconstruct its shape, which is—in this case—a rectangle. The higher-rank tensors thus obviously contain additional information. However, if we assume that the shape is a rectangle, then the second-rank tensor suffices to estimate the perimeter and the aspect ratio of the rectangle. This determines its shape, and thus, we can predict all higher-rank tensors. Interestingly, we can use these relations to test the assumption by comparing our predictions with the measured values.

In the same way, the relation between tensors of different rank that we found for Gaussian random fields can be used to detect non-Gaussianities in anisotropic random fields. Because the relation does not depend on the details of the model, that is, on the

correlation function of the Gaussian random field, it would be ideally suitable for a null hypothesis test. We discuss this outlook in the following section.

5. Conclusion and outlook to a robust detection of non-Gaussianities

We have shown that MTs detect and quantify anisotropy in random fields robustly and comprehensively; see, e.g., Fig. 2. Our simulations demonstrate that the asymptotic results are robust against noise and finite-size effects. Therefore, we are convinced that our shape analysis can be useful for experiments and applications in physics, where the Gaussian random field is already a common model; e.g., for rough surfaces [28, 29], porous media [26, 33], or as solutions to stochastic partial differential equations like the heat equation [64], but also for other fields of science and technology, including image processing, geostatistics, or spatial statistics.

Shape information encoded in MTs Importantly, we have carefully discussed the different geometrical information contained in tensors of different order (e.g., volume-based versus interfacial based MTs) and of different rank. For quite general random fields f (that are ergodic, sufficiently smooth and integrable), the volume tensors only contain the volume of the excursion set and shape information about the observation window, see Eq. (16). For the interfacial tensors, the global average of the MTs can be expressed in the thermodynamic limit by a local average of the functional value and the gradient at the origin, see Eq. (21). They are suitable to characterize the global anisotropy of ergodic random fields since they quantify the intrinsic anisotropy of the Gaussian random field (independent of the threshold).

Due to the symmetry of the Gaussian random field, all MT tensor densities $w_1^{0,2s-1}$ of odd rank vanish. For the even rank tensor densities, we derive an explicit integral expression for arbitrary dimensions, see Eq. (26). In two dimensions, we derive the explicit expression in Eq. (28). Comparing the analytic results to simulations, see Figure 2, we show how the MT densities detect anisotropy in the Gaussian random field and quantify the degree of anisotropy. We demonstrate this for a parametric model with a tunable degree of anisotropy, as described in Appendix A.

The irreducible representation of MTs reveals that tensors of different rank contain additional information about the anisotropy of the level sets, see Fig. 3; for an introduction to the irreducible representation, see Appendix B. The more tensors we determine, the more accurately the level sets are characterized without prior knowledge about the random field.

Perhaps surprisingly, we have shown that if we know the random field is Gaussian, then this additional information can be predicted from the second-rank tensor. This is because the essential information about the Gaussian random field encoded in the Minkowski tensors is a second rank tensor, the covariance matrix of the gradient at the origin, see Eq. (44). The second-rank tensor $w_1^{0,2}$ thus accesses all information from the Gaussian random field that is needed to determine the higher-rank tensors $w_1^{0,s}$ (once

we know that the random field is Gaussian).

Based on a measurement of $w_1^{0,2}$, we can estimate the EGI density, see Fig. 4, and thus all tensor densities $w_1^{0,s}$, see Eq. (45). Our simulations have demonstrated that a moderately large collection of samples with a relatively small system size is sufficient for a robust and accurate estimate.

Basis for a robust null hypothesis test Our relation between tensors of different rank provides the basis for a null hypothesis test detecting non-Gaussianities in anisotropic random spatial structures. First, the second-rank tensor is measured. Then its prediction of, e.g., the fourth-rank tensor can be compared to the measured value of the tensor of rank four. A statistically significant deviation of the prediction from the measurement would indicate a non-Gaussian contribution. Such a test could, for example, be constructed similar to the test on complete spatial randomness using Minkowski functionals in [10, 40].

A major advantage of such a test is the complete independence from the models of the Gaussian random field; essentially, we only assume integrability and smoothness as mentioned above. For a rigorous hypothesis test, the covariances of MTs and central limit theorems are needed, which were recently proven for the MFs in the thermodynamic limit [53, 54, 91], as well as for an average of interfacial MTs over all thresholds [91]. The exact values of the covariances will probably depend on the details of the model. Nevertheless, we expect that a null hypothesis test that detects non-Gaussianities in anisotropic random fields using MTs would be robust against minor changes in the model because the relation between the mean values of MTs is universal.

Acknowledgments

We are grateful to Maria Schlecht and Daniel Göring for their preliminary work on the shape of Gaussian random fields. We thank Dennis Müller for our insightful discussions. We thank Anne Estrade and Julie Fournier for stimulating discussions and Mark Dennis for pointing out the random waves model. M.A.K. and K.M. acknowledge support by the Deutsche Forschungsgemeinschaft (DFG) through the SPP 2265, under grant number ME 1361/16-1, and by the Volkswagenstiftung via the “Experiment” Project “Finite Projective Geometry.”

Appendix A. Parametric Gaussian random wave model

For our simulations, we use a parametric model of a Gaussian random field, where we can tune the degree of anisotropy and preferred orientation. Our model belongs to the class of Gaussian random wave models [4, 9, 92], which is an exemplary class of Gaussian random fields. These models are especially important in physics; for example, Gaussian random waves solve the time-independent Helmholtz wave equation [9] and are physically well-justified models for chaotic quantum systems [61, 93]. Moreover, they are

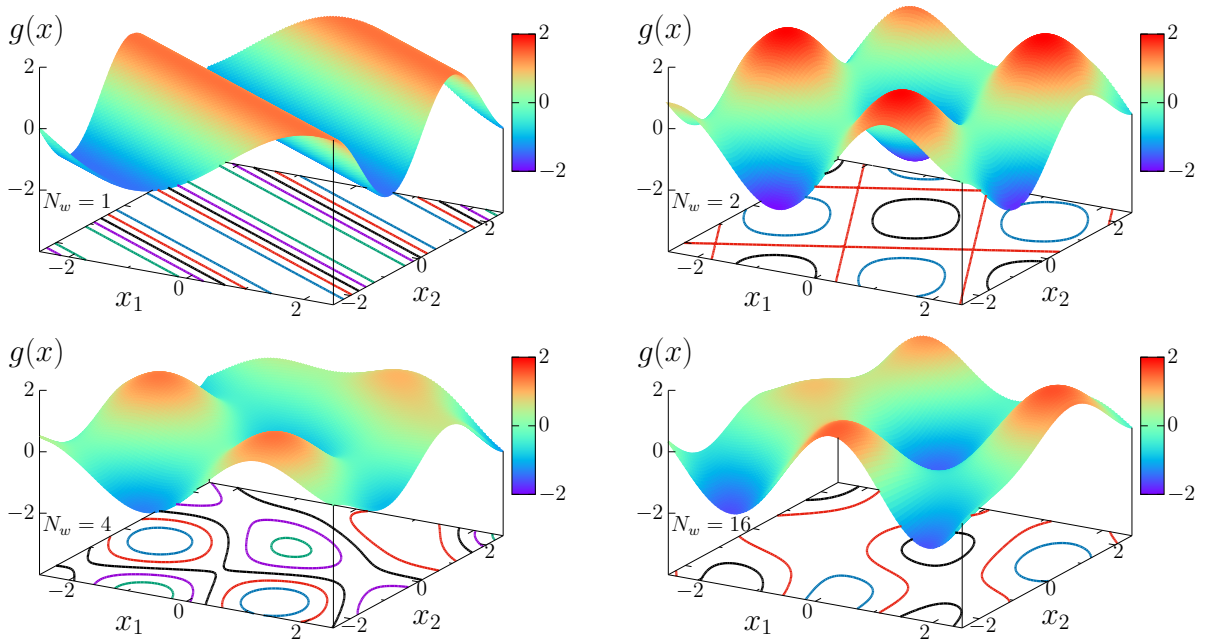


Figure A1. Gaussian random waves, see Eq. (A.1), the plots show the superposition of $N_w = 1, 2, 4, 16$ plain waves with random phases and orientation. It quickly converges to a Gaussian random field.

connected to optical speckle patterns [8, 25]. In contrast to the typical isotropic models, our model has, as mentioned above, a tunable degree of anisotropy. Our parametric model was first defined in [36] and has also been studied in [63].

The basic idea is to superimpose plane waves with random phases η_i and a random direction k_i of the wave vector:

$$g(x) = \sqrt{\frac{2}{N_w}} \sum_{i=1}^{N_w} \cos(k_i x + \eta_i), \quad (\text{A.1})$$

where the random phases η_i are uniformly distributed on $[0, 2\pi)$ and $\|k_i\| \equiv 1$. We note in passing that, by our choice that $\|k_i\| \equiv 1$, our Gaussian models are stealthy hyperuniform, i.e., they anomalously suppress density fluctuations on large scales [94–96]. Variants of our model can be used to construct Gaussian random fields that are only anisotropic in specific directions [46].

At each position x , the functional values of the random waves are independently and identically distributed random variables. Because of the central limit theorem, the superposition is, therefore, approximately a Gaussian random field for a large number N_w of random waves, where in our simulation, $N_w = 100$. Figure A1 shows the stepwise construction of our Gaussian random wave model for the sample in Fig. 1. The distribution of k_i on \mathbb{S}^{d-1} controls the anisotropy of the system. The model is isotropic for a uniform distribution on \mathbb{S}^{d-1} . It is anisotropic if there is an orientation bias in the distribution of k_i .

Here we describe a two-dimensional model, where we parametrize the direction $k_i \in \mathbb{S}^1$ by the angle θ_i between k_i and the x -axis. We choose for the probability density

of θ (similar to the anisotropic distributions in [34, 45, 71, 97]):

$$f_\alpha(\theta) = Z_\alpha \cos^\alpha(\theta) \quad (\text{A.2})$$

with $Z_\alpha = \Gamma(1 + \alpha/2)/(\sqrt{\pi}\Gamma(1/2 + \alpha/2))$ with $\theta \in (-\pi/2, \pi/2]$. The parameter α varies the anisotropy from perfect alignment ($\alpha = \infty$) to an isotropic distribution ($\alpha = 0$). Interestingly, for fixed $\alpha = 1$, the anisotropic Gaussian random waves can model polarized light fields [98].

The power spectral density $s(q)$ follows directly from the multivariate probability density function of k_i :

$$s(q) = 2\pi^2 \delta(\|q\| - 1) Z_\alpha |\cos(\theta)|^\alpha, \quad (\text{A.3})$$

where $\theta \in [-\pi, \pi)$ is the angle between q and the x -axis. In contrast to the orientation distribution in Eq. (A.2), $Z_\alpha |\cos(\theta)|^\alpha$ is defined for all directions.

The eigenvalues λ_1 and λ_2 of the covariance matrix $\text{Cov}[\nabla g(0)]$ of the gradient of g at the origin are

$$\lambda_1 = \frac{1 + \alpha}{2 + \alpha} \quad \text{and} \quad \lambda_2 = \frac{1}{2 + \alpha}, \quad (\text{A.4})$$

and depend as expected on the anisotropy of the model. In the limit $\alpha \rightarrow \infty$, all wave vectors are aligned in the same direction, i.e., all wavefronts are parallel to each other. The model becomes an effectively one-dimensional random field that is simply extended perpendicular to the wavefronts. Accordingly for $\alpha \rightarrow \infty$, $\lambda_1 \rightarrow 1$ and $\lambda_2 \rightarrow 0$. In the isotropic case, $\alpha = 0$, the eigenvalues coincide $\lambda_1 = \lambda_2 = 1/2$.

We simulate for each parameter $\alpha = 0, 1, 3$, 1000 samples within the observation window $[0, 20]^2$ for Figs. 2 and 3, and 2000 samples for Fig. 4. In our simulation, we first sample the parameters of the function $g(x)$ in Eq. (A.1). At each threshold, we approximate the level set by a polygon, using the software `GNU PLOT`, for which the MTs and EGI can quickly be evaluated using a `PYTHON` script. To sample the random numbers, we use the `MT19937` generator, which is known as the ‘‘Mersenne Twister’’, implemented in the `BOOST LIBRARIES`.

Appendix B. Irreducible representation of Minkowski tensors

An irreducible representation of Minkowski tensors in two dimensions provides convenient access to anisotropy information of high-rank tensors. Importantly, such an irreducible representation avoids redundant information in tensors of different rank. In that sense, the irreducible representation of a tensor of rank s is the anisotropy information that is exclusive to this rank. This is in contrast to the Cartesian representation, where the definition is intuitive but where the same information can be contained in tensors of different rank.

We decompose the Minkowski tensors into irreducible tensors with respect to the rotation group $\text{SO}(d)$; see [99] for a discussion of irreducible representations of moment tensors of the directional distributions and [100] for a general theory of an irreducible decomposition of the space of translational-invariant and continuous valuations. For

three dimensions, an explicit irreducible representation and rotational invariants of Minkowski tensors are presented in [101–103]. Here, the two-dimensional case of *irreducible Minkowski tensors* (IMTs) for the interfacial tensors $W_1^{0,s}$ for a convex body K is discussed; see also [11, 71]. Note that the IMTs are equivalent to the definition of the harmonic intrinsic volumes defined in [104].

Here we provide an intuitive approach to the IMTs based on an interpretation of $W_1^{0,s}$ as being essentially moment tensors of the normals on the interface of a domain K :

$$W_1^{0,s}(K) = \int_{\partial K} n^s(x) dS(x) \quad (\text{B.1})$$

$$= \int_{\partial K} \int_{\mathbb{S}^{d-1}} u^s \delta(n(x) - u) du dS(x) \quad (\text{B.2})$$

$$= \int_{\mathbb{S}^{d-1}} u^s \int_{\partial K} \delta(n(x) - u) dS(x) du \quad (\text{B.3})$$

$$= \int_{\mathbb{S}^{d-1}} u^s \Psi_K(u) du, \quad (\text{B.4})$$

where

$$\Psi_K(u) := \int_{\partial K} \delta(n(x) - u) dS(x) \quad (\text{B.5})$$

is the so-called *extended Gaussian image* (EGI) [105]. It is defined on the unit sphere (or circle in $d = 2$) \mathbb{S}^{d-1} and is proportional to the probability density function of the normal vectors, but its normalization is equal to the surface area (or perimeter in $d = 2$) $W_1(K) = \int_{\mathbb{S}^1} \Psi_K(u) du$.

In two dimensions, the direction $u \in \mathbb{S}^1$ can be identified by the angle θ between u and the x -axis. Then $\Psi_K(\theta)$ is a periodic function on $[0, 2\pi)$ and can be represented by a Fourier series

$$\Psi_K(\theta) = \sum_{s=-\infty}^{\infty} \psi_s(K) e^{is\theta}, \text{ with} \quad (\text{B.6})$$

$$\psi_s(K) := \frac{1}{2\pi} \int_0^{2\pi} \Psi_K(\theta) e^{-is\theta} d\theta, \quad (\text{B.7})$$

so that $\psi_{-s}(K) = \psi_s^*(K)$. Because $e^{is\theta}$ with $s \in \mathbb{Z}$ are the irreducible representations of $\text{SO}(2)$, the Fourier coefficients $\psi_s(K)$ of the EGI are the IMTs, that is, the irreducible representations of the translation invariant interfacial tensors $W_1^{0,s}(K)$. For a rotation of K by an angle β , i.e., $\Psi_K(\theta) \rightarrow \Psi_K(\theta - \beta)$, we obtain for the IMTs the simple transformations

$$\psi_s(K) \rightarrow e^{-is\beta} \psi_s(K). \quad (\text{B.8})$$

Hence, the phase of the complex number $\psi_s(K)$ contains information about the preferred direction. Its absolute value $|\psi_s(K)|$ is a scalar index (or rotational invariant). For $s = 0$, $\psi_0(K) = W_1/(2\pi)$, and $\psi_{\pm 1}(K) = 0$ for a closed body K . For $|s| \geq 2$, $|\psi_s(K)|$ quantifies the degree of anisotropy. Hence, we define the anisotropy indices

$$q_s(K) := \frac{|\psi_s(K)|}{\psi_0(K)} \in [0, 1], \quad (\text{B.9})$$

which are unit free. For $s \geq 2$, $q_s(K)$ measures the degree of anisotropy of rank s , i.e., isotropy results in $q_s(K) = 0$, and $q_s(K) = 1$ indicates maximal interfacial anisotropy. The anisotropy index $q_2(K)$ can be expressed by the eigenvalues $\delta_1(K)$ and $\delta_2(K)$ of the Minkowski tensor $W_1^{0,2}(K)$ in the Cartesian representation:

$$q_2(K) = \frac{|\delta_1(K) - \delta_2(K)|}{\delta_1(K) + \delta_2(K)}. \quad (\text{B.10})$$

The fourth-rank index $q_4(K)$ can also be conveniently expressed by the components of the Minkowski tensor $W_1^{0,4}(K)$ if the coordinate axes are assumed to coincide with the main axes of the system (i.e. the eigenvectors of $W_1^{0,2}(K)$):

$$q_4(K) = \frac{|(W_1^{0,4}(K))_{xxxx} + (W_1^{0,4}(K))_{yyyy} - 6(W_1^{0,4}(K))_{xxyy}|}{(W_1^{0,4}(K))_{xxxx} + (W_1^{0,4}(K))_{yyyy} + 2(W_1^{0,4}(K))_{xxyy}}. \quad (\text{B.11})$$

We derive these relations by expressing the Cartesian Minkowski tensors via IMTs:

$$W_1^{0,s}(K) = \int_{\mathbb{S}^1} u^s \Psi_K(u) du = \sum_{t=-s}^s \psi_t(K) \int_0^{2\pi} u^s(\theta) e^{it\theta} d\theta, \quad (\text{B.12})$$

where the last equality holds because all terms with $|t| > s$ vanish because of the vanishing the Fourier components of u^s . Equation (B.12) contains the Fourier coefficients of $u^s(\theta)$, which are independent of the domain K . For $s = 2$, for example, they are given by

$$\int_0^{2\pi} u^2(\theta) e^{is\theta} d\theta = \begin{cases} \pi \mathbf{1} & \text{if } s = 0, \\ \frac{\pi}{2} (\sigma_3 + i\sigma_1) & \text{if } s = 2, \\ \frac{\pi}{2} (\sigma_3 - i\sigma_1) & \text{if } s = -2, \\ \mathbb{O} & \text{else,} \end{cases} \quad (\text{B.13})$$

where $\mathbf{1}$ is the unit tensor, \mathbb{O} the zero tensor, and σ_j are Pauli matrices with

$$\sigma_3 = \begin{pmatrix} 1 & 0 \\ 0 & -1 \end{pmatrix} \quad \text{and} \quad \sigma_1 = \begin{pmatrix} 0 & 1 \\ 1 & 0 \end{pmatrix}.$$

Thus, $W_1^{0,2}(K)$ can be expressed by $\psi_0(K)$, $\psi_1(K)$, and $\psi_2(K)$, and vice versa. From

$$W_1^{0,2}(K) = \psi_0(K) \pi \mathbf{1} + \psi_2(K) \frac{\pi}{2} (\sigma_3 + i\sigma_1) + \psi_{-2}(K) \frac{\pi}{2} (\sigma_3 - i\sigma_1) \quad (\text{B.14})$$

$$= \psi_0(K) \pi \mathbf{1} + \text{Re}[\psi_2(K)] \pi \sigma_3 - \text{Im}[\psi_2(K)] \pi \sigma_1 \quad (\text{B.15})$$

follows that

$$\psi_0(K) = \frac{1}{2\pi} ((W_1^{0,2}(K))_{xx} + (W_1^{0,2}(K))_{yy}) = \frac{1}{2\pi} W_1(K), \quad (\text{B.16})$$

$$\text{Re}[\psi_2(K)] = \frac{1}{2\pi} ((W_1^{0,2}(K))_{xx} - (W_1^{0,2}(K))_{yy}), \quad (\text{B.17})$$

$$\text{Im}[\psi_2(K)] = -\frac{1}{\pi} (W_1^{0,2}(K))_{xy}. \quad (\text{B.18})$$

References

- [1] Robert J. Adler and Jonathan E. Taylor. *Random Fields and Geometry*. Springer Monographs in Mathematics. Springer, New York, 2007.
- [2] S. N. Chiu, D. Stoyan, W. S. Kendall, and J. Mecke. *Stochastic Geometry and Its Applications*. Wiley, Chichester, third edition, 2013.
- [3] Erik Vanmarcke. *Random Fields: Analysis and Synthesis*. World Scientific, 2010.
- [4] M V Berry. Regular and irregular semiclassical wavefunctions. *J. Phys. Math. Gen.*, 10:2083–2091, 1977.
- [5] P. J. E. Peebles. *Principles of Physical Cosmology*. Princeton University Press, Princeton, NJ, 1993.
- [6] Salvatore Torquato. *Random Heterogeneous Materials*, volume 16 of *Interdisciplinary Applied Mathematics*. Springer, New York, second edition, 2002.
- [7] Andrew R. Liddle and D. H. Lyth. *Cosmological Inflation and Large-Scale Structure*. Cambridge University Press, Cambridge, U.K. ; New York, 2000.
- [8] J. W. Goodman. *Speckle Phenomena in Optics: Theory and Applications*. Roberts & Company, Greenwood Village, 2007.
- [9] M. R. Dennis. Nodal densities of planar gaussian random waves. *Eur. Phys. J. Spec. Top.*, 145:191–210, 2007.
- [10] Michael A. Klatt and Klaus Mecke. Detecting structured sources in noisy images via Minkowski maps. *EPL*, 128:60001, 2019.
- [11] Caroline Collischon, Manami Sasaki, Klaus Mecke, Sean D. Points, and Michael A. Klatt. Tracking down the origin of superbubbles and supergiant shells in the Magellanic Clouds with Minkowski tensor analysis. *A&A*, 653:A16, 2021.
- [12] Christian Scholz, Frank Wirner, Michael A. Klatt, Daniel Hirneise, Gerd E. Schröder-Turk, Klaus Mecke, and Clemens Bechinger. Direct relations between morphology and transport in Boolean models. *Phys. Rev. E*, 92:043023, 2015.
- [13] B. Schuetrumpf, M. A. Klatt, K. Iida, G. E. Schröder-Turk, J. A. Maruhn, K. Mecke, and P.-G. Reinhard. Appearance of the single gyroid network phase in “nuclear pasta” matter. *Phys. Rev. C*, 91:025801, 2015.
- [14] Hideyuki Mizuno, Leonardo E. Silbert, and Matthias Sperl. Spatial Distributions of Local Elastic Moduli Near the Jamming Transition. *Phys. Rev. Lett.*, 116:068302, 2016.
- [15] Yuanjian Zheng, Anshul D. S. Parmar, and Massimo Pica Ciamarra. Hidden Order Beyond Hyperuniformity in Critical Absorbing States. *Phys. Rev. Lett.*, 126:118003, 2021.
- [16] Yang Jiao. Hyperuniformity of expected equilibrium density distributions of Brownian particles via designer external potentials. *Physica A: Statistical Mechanics and its Applications*, page 126435, 2021.
- [17] David J. Whitehouse. Surface Characterization and Roughness Measurement in Engineering. In Pramod K. Rastogi, editor, *Photomechanics*, Topics in Applied Physics, pages 413–461. Springer, Berlin, Heidelberg, 2000.
- [18] Xingchen Ji, Felipe A. S. Barbosa, Samantha P. Roberts, Avik Dutt, Jaime Cardenas, Yoshitomo Okawachi, Alex Bryant, Alexander L. Gaeta, and Michal Lipson. Ultra-low-loss on-chip resonators with sub-milliwatt parametric oscillation threshold. *Optica*, 4:619, 2017.
- [19] Christian Spengler, Friederike Nolle, Johannes Mischo, Thomas Faidt, Samuel Grandthyll, Nicolas Thewes, Marcus Koch, Frank Müller, Markus Bischoff, Michael Andreas Klatt, and Karin Jacobs. Strength of bacterial adhesion on nanostructured surfaces quantified by substrate morphometry. *Nanoscale*, 11:19713–19722, 2019.
- [20] M. V. Berry and M. R. Dennis. Phase singularities in isotropic random waves. *P Roy Soc -Math Phy*, 456:2059, 2000.
- [21] Keiichi Edagawa, Satoshi Kanoko, and Masaya Notomi. Photonic Amorphous Diamond Structure with a 3D Photonic Band Gap. *Phys. Rev. Lett.*, 100:013901, 2008.

- [22] Michael A. Klatt, Paul J. Steinhardt, and Salvatore Torquato. Gap Sensitivity Reveals Universal Behaviors in Optimized Photonic Crystal and Disordered Networks. *Phys. Rev. Lett.*, 127:037401, 2021.
- [23] Robert J. Adler. *The Geometry of Random Fields*. SIAM, 1981.
- [24] M. V. Berry. Statistics of nodal lines and points in chaotic quantum billiards: Perimeter corrections, fluctuations, curvature. *J. Phys. A: Math. Gen.*, 35:3025, 2002.
- [25] J. W. Goodman. *Statistical Optics*. Wiley, New York, 1985.
- [26] M. Teubner. Level surfaces of Gaussian random fields and microemulsions. *EPL Europhys. Lett.*, 14:403, 1991.
- [27] H. Mantz, K. Jacobs, and K. Mecke. Utilising Minkowski Functionals for Image Analysis. *J Stat Mech*, 12:P12015, 2008.
- [28] R. Filliger, O. Mermoud, D. Trivun, and P. Walther. 3D anisotropy measurement methodology for surface microstructures: 3D anisotropy measurement methodology for surface microstructures. *Surf. Interface Anal.*, 44:1547–1557, 2012.
- [29] Matthias Lessel, Peter Loskill, Florian Hausen, Nitya Nand Gosvami, Roland Bennewitz, and Karin Jacobs. Impact of van der Waals Interactions on Single Asperity Friction. *Phys. Rev. Lett.*, 111:035502, 2013.
- [30] Jürgen Becker, Günther Grün, Ralf Seemann, Hubert Mantz, Karin Jacobs, Klaus R. Mecke, and Ralf Blossey. Complex dewetting scenarios captured by thin-film models. *Nat. Mater.*, 2:59–63, 2003.
- [31] M. S. Longuet-Higgins. The statistical analysis of a random, moving surface. *Phil Trans R Soc Lond A*, 249:321–387, 1957.
- [32] A. P. Roberts and Max Teubner. Transport properties of heterogeneous materials derived from Gaussian random fields: Bounds and simulation. *Phys. Rev. E*, 51:4141, 1995.
- [33] A. P. Roberts and S. Torquato. Chord-distribution functions of three-dimensional random media: Approximate first-passage times of Gaussian processes. *Phys. Rev. E*, 59:4953–4963, 1999.
- [34] G. E. Schröder-Turk, W. Mickel, S. C. Kapfer, M. A. Klatt, F. M. Schaller, M. J. F. Hoffmann, N. Kleppmann, P. Armstrong, A. Inayat, D. Hug, M. Reichelsdorfer, W. Peukert, W. Schwieger, and K. Mecke. Minkowski Tensor Shape Analysis of Cellular, Granular and Porous Structures. *Adv. Mater.*, 23:2535–2553, 2011.
- [35] R. Schneider and W. Weil. *Stochastic and Integral Geometry (Probability and Its Applications)*. Springer, Berlin, 2008.
- [36] Michael A. Klatt. *Morphometry of Random Spatial Structures in Physics*. PhD thesis, Friedrich-Alexander-Universität Erlangen-Nürnberg, Erlangen, 2016.
- [37] M. Kerscher, K. Mecke, J. Schmalzing, C. Beisbart, T. Buchert, and H. Wagner. Morphological fluctuations of large-scale structure: The PSCz survey. *A&A*, 373:1–11, 2001.
- [38] D. Göring, M. A. Klatt, C. Stegmann, and K. Mecke. Morphometric analysis in gamma-ray astronomy using Minkowski functionals: Source detection via structure quantification. *Astron. Astrophys.*, 555:A38, 2013.
- [39] B. Schuetrumpf, M. A. Klatt, K. Iida, J. A. Maruhn, K. Mecke, and P.-G. Reinhard. Time-dependent Hartree-Fock approach to nuclear “pasta” at finite temperature. *Phys. Rev. C*, 87:055805, 2013.
- [40] Bruno Ebner, Norbert Henze, Michael A. Klatt, and Klaus Mecke. Goodness-of-fit tests for complete spatial randomness based on Minkowski functionals of binary images. *Electron. J. Statist.*, 12:2873–2904, 2018.
- [41] K. R. Mecke, Th. Buchert, and H. Wagner. Robust morphological measures for large-scale structure in the universe. *Astron Astrophys*, 288:697, 1994.
- [42] Marconi Barbosa, Riccardo Natoli, Kriztina Valter, Jan Provis, and Ted Maddess. Integral-geometry characterization of photobiomodulation effects on retinal vessel morphology. *Biomed. Opt. Express*, BOE, 5:2317–2332, 2014.
- [43] C. R ath, R. Monetti, J. Bauer, I. Sidorenko, D. M uller, M. Matsuura, E.-M. Lochm uller,

- P. Zysset, and F. Eckstein. Strength through structure: Visualization and local assessment of the trabecular bone structure. *New J. Phys.*, 10:125010, 2008.
- [44] C.H. Arns, M.A. Knackstedt, and K. Mecke. 3D structural analysis: Sensitivity of Minkowski functionals: 3D STRUCTURAL ANALYSIS: SENSITIVITY OF MINKOWSKI FUNCTIONALS. *J. Microsc.*, 240:181–196, 2010.
- [45] Michael A Klatt, Gerd E Schröder-Turk, and Klaus Mecke. Anisotropy in finite continuum percolation: Threshold estimation by Minkowski functionals. *J. Stat. Mech. Theor. Exp.*, 2017:023302, 2017.
- [46] Salvatore Torquato. Hyperuniformity and its generalizations. *Phys. Rev. E*, 94:022122, 2016.
- [47] Alexander J. Taylor and Mark R. Dennis. Vortex knots in tangled quantum eigenfunctions. *Nat. Commun.*, 7:12346, 2016.
- [48] Hiroyuki Tomita. Statistical properties of random interface system. *Prog. Theor. Phys.*, 75:482–495, 1986.
- [49] Anne Estrade and José R. León. A central limit theorem for the Euler characteristic of a Gaussian excursion set. *Ann. Probab.*, 44:3849–3878, 2016.
- [50] Domenico Marinucci, Giovanni Peccati, Maurizia Rossi, and Igor Wigman. Non-Universality of Nodal Length Distribution for Arithmetic Random Waves. *Geom. Funct. Anal.*, 26:926–960, 2016.
- [51] Valentina Cammarota and Domenico Marinucci. A Quantitative Central Limit Theorem for the Euler-Poincaré Characteristic of Random Spherical Eigenfunctions. *ArXiv160309588 Math*, 2016.
- [52] Ivan Nourdin, Giovanni Peccati, and Maurizia Rossi. Nodal Statistics of Planar Random Waves. *ArXiv170802281 Math-Ph*, 2017.
- [53] D. Müller. A central limit theorem for Lipschitz–Killing curvatures of Gaussian excursions. *J. Math. Anal. Appl.*, 452:1040–1081, 2017.
- [54] M. Kratz and S. Vadlamani. Central Limit Theorem for Lipschitz–Killing Curvatures of Excursion Sets of Gaussian Random Fields. *J. Theor. Probab.*, pages 1–30, 2017.
- [55] Elena Di Bernardino, Anne Estrade, and José R. León. A test of Gaussianity based on the Euler characteristic of excursion sets. *Electron. J. Stat.*, 11:843–890, 2017.
- [56] Jens Schmalzing, Thomas Buchert, Adrian L. Melott, Varun Sahni, B. S. Sathyaprakash, and Sergei F. Shandarin. Disentangling the Cosmic Web. I. Morphology of Isodensity Contours. *Astrophys J*, 526:568, 1999.
- [57] Christoph Räth and Peter Schuecker. Analysing large-scale structure II. Testing for primordial non-Gaussianity in CMB maps using surrogates. *Mon. Not. R. Astron. Soc.*, 344:115–128, 2003.
- [58] A. Ducout, F. R. Bouchet, S. Colombi, D. Pogosyan, and S. Prunet. Non-Gaussianity and Minkowski functionals: Forecasts for Planck. *Mon Not R Astron Soc*, 429:2104–2126, 2013.
- [59] C. P. Novaes, A. Bernui, G. A. Marques, and I. S. Ferreira. Local analyses of Planck maps with Minkowski functionals. *Monthly Notices of the Royal Astronomical Society*, 461:1363–1373, 2016.
- [60] Planck Collaboration. Planck 2018 results. VII. Isotropy and statistics of the CMB. *Astron. Astrophys.*, 641:A7, 2020.
- [61] Juan Diego Urbina and Klaus Richter. Supporting random wave models: A quantum mechanical approach. *J. Phys. A: Math. Gen.*, 36:L495, 2003.
- [62] Aline Bonami and Anne Estrade. Anisotropic analysis of some gaussian models. *J. Fourier Anal. Appl.*, 9:215, 2003.
- [63] Anne Estrade and Julie Fournier. Anisotropic Gaussian wave models. *ALEA*, 17:329, 2020.
- [64] Yimin Xiao. Sample path properties of anisotropic gaussian random fields. In Davar Khoshnevisan and Firas Rassoul-Agha, editors, *A Minicourse on Stochastic Partial Differential Equations*, pages 145–212. Springer, Berlin, Heidelberg, 2009.
- [65] Dan Cheng and Yimin Xiao. The mean Euler characteristic and excursion probability of Gaussian

- random fields with stationary increments. *Ann. Appl. Probab.*, 26:722–759, 2016.
- [66] Frédéric Richard and Hermine Bierme. Statistical Tests of Anisotropy for Fractional Brownian Textures. Application to Full-field Digital Mammography. *J. Math. Imaging Vis.*, 36:227–240, 2010.
- [67] P. McMullen. Isometry covariant valuations on convex bodies. *Rend. Circ. Mat. Palermo (2) Suppl.*, 50:259–271, 1997.
- [68] Michael A. Klatt, Günter Last, Klaus Mecke, Claudia Redenbach, Fabian M. Schaller, and Gerd E. Schröder-Turk. Cell Shape Analysis of Random Tessellations Based on Minkowski Tensors. In Eva B. Vedel Jensen and Markus Kiderlen, editors, *Tensor Valuations and Their Applications in Stochastic Geometry and Imaging*, volume 2177 of *Lecture Notes in Mathematics*, pages 385–421. Springer International Publishing, Cham, 2017.
- [69] A. Böbel and C. Räh. Kinetics of fluid demixing in complex plasmas: Domain growth analysis using Minkowski tensors. *Phys Rev E*, 94:013201, 2016.
- [70] Michael A. Klatt, Gerd E. Schröder-Turk, and Klaus Mecke. Mean-intercept anisotropy analysis of porous media. I. Analytic formulae for anisotropic Boolean models. *Med. Phys.*, 44:3650–3662, 2017.
- [71] Michael A. Klatt, Gerd E. Schröder-Turk, and Klaus Mecke. Mean-intercept anisotropy analysis of porous media. II. Conceptual shortcomings of the MIL tensor definition and Minkowski tensors as an alternative. *Med. Phys.*, 44:3663–3675, 2017.
- [72] M. Saadatfar, M. Mukherjee, M. Madadi, G. E. Schröder-Turk, F. Garcia-Moreno, F. M. Schaller, S. Hutzler, A. P. Sheppard, J. Banhart, and U. Ramamurty. Structure and deformation correlation of closed-cell aluminium foam subject to uniaxial compression. *Acta Materialia*, 60:3604–3615, 2012.
- [73] G. E. Schröder-Turk, W. Mickel, S. C. Kapfer, F. M. Schaller, B. Breidenbach, D. Hug, and K. Mecke. Minkowski tensors of anisotropic spatial structure. *New J. Phys.*, 15:083028, 2013.
- [74] Fabian M. Schaller, Sebastian C. Kapfer, James E. Hilton, Paul W. Cleary, Klaus Mecke, Cristiano De Michele, Tanja Schilling, Mohammad Saadatfar, Matthias Schröter, Gary W. Delaney, and Gerd E. Schröder-Turk. Non-universal Voronoi cell shapes in amorphous ellipsoid packs. *Eur. Lett.*, 111:24002, 2015.
- [75] Chengjie Xia, Jindong Li, Yixin Cao, Binqun Kou, Xianghui Xiao, Kamel Fezzaa, Tiqiao Xiao, and Yujie Wang. The structural origin of the hard-sphere glass transition in granular packing. *Nat. Commun.*, 6:8409, 2015.
- [76] Simon Weis and Matthias Schröter. Analyzing X-ray tomographies of granular packings. *Rev. Sci. Instrum.*, 88:051809, 2017.
- [77] Pravabati Chingangbam, K. P. Yogendran, P. K. Joby, Vidhya Ganesan, Stephen Appleby, and Changbom Park. Tensor Minkowski Functionals for random fields on the sphere. *J. Cosmol. Astropart. Phys.*, 2017:023, 2017.
- [78] Akanksha Kapahtia, Pravabati Chingangbam, Stephen Appleby, and Changbom Park. A novel probe of bubble size statistics and time scales of the epoch of reionization using the contour Minkowski Tensor. *ArXiv Prepr. ArXiv171209195*, 2017.
- [79] Vidhya Ganesan and Pravabati Chingangbam. Tensor Minkowski Functionals: First application to the CMB. *J. Cosmol. Astropart. Phys.*, 2017:023–023, 2017.
- [80] Stephen Appleby, Pravabati Chingangbam, Changbom Park, Sungwook E. Hong, Juhan Kim, and Vidhya Ganesan. Minkowski Tensors in Two Dimensions - Probing the Morphology and Isotropy of the Matter and Galaxy Density Fields. *ArXiv171207466 Astro-Ph*, 2017.
- [81] Stephen Appleby, Pravabati Chingangbam, Changbom Park, K. P. Yogendran, and P. K. Joby. Minkowski Tensors in Three Dimensions: Probing the Anisotropy Generated by Redshift Space Distortion. *ApJ*, 863:200, 2018.
- [82] Pravabati Chingangbam, Priya Goyal, K. P. Yogendran, and Stephen Appleby. The geometrical meaning of statistical isotropy of smooth random fields in two dimensions. *ArXiv210905726 Astro-Ph*, 2021.

- [83] Max Hörmann. *Minkowski Tensors of Gaussian Fields*. Bachelor's thesis, Friedrich-Alexander-Universität Erlangen-Nürnberg (FAU), 2014.
- [84] Jürgen Potthoff. Sample properties of random fields III: Differentiability. *Commun. Stoch. Anal.*, 4:3, 2010.
- [85] Zoltán Sasvári. *Multivariate Characteristic and Correlation Functions*. De Gruyter, Berlin, Boston, 2013.
- [86] H. Hadwiger. *Vorlesungen Über Inhalt, Oberfläche Und Isoperimetrie*. Springer, Berlin, 1957.
- [87] Semyon Alesker. Continuous rotation invariant valuations on convex sets. *Ann. Math.*, 149:977, 1999.
- [88] S. Alesker. Description of Continuous Isometry Covariant Valuations on Convex Sets. *Geometriae Dedicata*, 74:241–248, 1999.
- [89] Daniel Hug and Rolf Schneider. Tensor Valuations and Their Local Versions. In Eva B. Vedel Jensen and Markus Kiderlen, editors, *Tensor Valuations and Their Applications in Stochastic Geometry and Imaging*, volume 2177 of *Lecture Notes in Mathematics*, pages 27–65. Springer International Publishing, Cham, 2017.
- [90] E. B. Vedel Jensen. *Local Stereology*. Advanced Series on Statistical Science & Applied Probability. World Scientific, Singapore, 1998.
- [91] D. Müller. *Central Limit Theorems for Geometric Functionals of Gaussian Excursion Sets*. PhD thesis, Karlsruhe Institute of Technology, 2018 (to be submitted).
- [92] N. F. Berk. Scattering properties of the leveled-wave model of random morphologies. *Phys. Rev. A*, 44:5069–5079, 1991.
- [93] Arnd Bäcker and Roman Schubert. Autocorrelation function of eigenstates in chaotic and mixed systems. *J. Phys. A: Math. Gen.*, 35:539, 2002.
- [94] Salvatore Torquato and Frank H. Stillinger. Local density fluctuations, hyperuniformity, and order metrics. *Phys. Rev. E*, 68:041113, 2003.
- [95] Zheng Ma and Salvatore Torquato. Random scalar fields and hyperuniformity. *Journal of Applied Physics*, 121:244904, 2017.
- [96] Salvatore Torquato. Hyperuniform states of matter. *Phys. Rep.*, 745:1–95, 2018.
- [97] Julia Hörrmann, Daniel Hug, Michael Andreas Klatt, and Klaus Mecke. Minkowski tensor density formulas for Boolean models. *Adv. Appl. Math.*, 55:48–85, 2014.
- [98] L. De Angelis, F. Alpeggiani, A. Di Falco, and L. Kuipers. Spatial Distribution of Phase Singularities in Optical Random Vector Waves. *Phys. Rev. Lett.*, 117:093901, 2016.
- [99] Ken-Ichi Kanatani. Distribution of directional data and fabric tensors. *Int. J. Eng. Sci.*, 22:149, 1984.
- [100] Semyon Alesker, Andreas Bernig, and Franz E. Schuster. Harmonic analysis of translation invariant valuations. *Geom. Funct. Anal.*, 21:751, 2011.
- [101] Sebastian C. Kapfer. *Morphometry and Physics of Particulate and Porous Media*. PhD thesis, Friedrich-Alexander-Universität Erlangen-Nürnberg, 2011.
- [102] Sebastian C. Kapfer, Walter Mickel, Klaus Mecke, and Gerd E. Schröder-Turk. Jammed spheres: Minkowski tensors reveal onset of local crystallinity. *Phys Rev E*, 85:030301, 2012.
- [103] Walter Mickel, Sebastian C. Kapfer, Gerd E. Schröder-Turk, and Klaus Mecke. Shortcomings of the bond orientational order parameters for the analysis of disordered particulate matter. *J. Chem. Phys.*, 138, 2013.
- [104] Julia Hörrmann. *The Method of Densities for Non-Isotropic Boolean Models*. KIT Scientific Publishing, Karlsruhe, 2015.
- [105] B.K.P. Horn. Extended Gaussian images. *Proc. IEEE*, 72:1671–1686, 1984.